Rock Mechanics and Rock Engineering (2021) 54:6299–6321
https://doi.org/10.1007/s00603-021-02614-9

ORIGINAL PAPER

# Time Series Prediction of Microseismic Multi-parameter Related to Rockburst Based on Deep Learning

Hang Zhang[1] · Jun Zeng[1] · Jiaji Ma[1] · Yong Fang[2] · Chunchi Ma[1,2] · Zhigang Yao[2] · Ziquan Chen[2]

Received: 7 March 2021 / Accepted: 6 August 2021 / Published online: 21 August 2021


## Abstract

Time series prediction refers to the learning of existing observed data of a parameter and predicting its future evolution. Based on the application of machine/deep learning methods in the field of engineering geology, it is desirable to predict the time series evolution of microseismic parameters in the process of rockburst development. Our study explores key microseismic indices that help describe the development process of rockbursts based on abundant rockburst data obtained from deep underground engineering construction. The integrated process of dynamic moving-window method and improved convolutional neural network (CNN) realizes the evolution prediction of multiple microseismic parameters or their different combinations, and the modified model structures of a univariate, multivariate input and a single-step, multi-step output are established. Various models of the multiple microseismic parameters for the CNN-based time series prediction are innovated, including a univariate prediction model, a multiple parallel series model, a multiple input series model, and a multivariate multi-step prediction model. Model training, testing, and interpretation of the rockburst risk and comparative analyses of the different models are performed for the complete process of multiple rockbursts. The results show that the proposed models can well predict the evolution trends in the various key characteristics during rockbursts. The predicted trend of multiple microseismic parameters provides time labels for rockburst prediction and risk judgement, which is conducive to rockburst early warning. This study provides a new research idea for the prediction and early warning of rockbursts in the field of deep underground and mining engineering.

**Keywords** Engineering geology · Rockburst risk · Microseismic parameter · Time series prediction · Deep learning method

✉ Yong Fang
fy980220@swjtu.cn

✉ Chunchi Ma
machunchi17@cdut.edu.cn

Hang Zhang
zhanghang@stu.cdut.edu.cn

Jun Zeng
1551010469@qq.com

Jiaji Ma
1812674679@qq.com

Zhigang Yao
bk20110739@my.swjtu.edu.cn

Ziquan Chen
196218337@qq.com

[1] State Key Laboratory of Geohazard Prevention and Geoenvironment Protection, Chengdu University of Technology, Chengdu 610059, Sichuan, China

[2] Key Laboratory of Transportation Tunnel Engineering, Ministry of Education, Southwest Jiaotong University, Chengdu 610031, Sichuan, China

## 1 Introduction

The construction of underground infrastructure and the exploitation of underground resources require venturing further deep into the earth. With the increasing complexity of deep geological environments and higher geo-stress levels, deep underground engineering projects have seen rockbursts that seriously impact construction and production safety (Li et al. 2019a, b; Feng et al. 2019, 2021; Liu et al. 2019; Zhang et al. 2020a, b, c, d). The microseismic monitoring technology used in this field can help continuously monitor and obtain the elastic waves of surrounding rock fractures for 24 h. The changes in the surrounding rock mechanics and fracture behavior can be described using the quantitative source theory, i.e., the time series law of microseismic parameters, so as to judge the risk of rockbursts (Liu et al. 2017a; De Santis et al. 2019; Li et al. 2019a, b; Kumar et al. 2019; Xiao et al. 2019; Dip et al. 2021). Thus, the microseismic monitoring technology can be used

to reveal the mechanism and characteristics of rockbursts, providing an effective tool for their interpretation and evaluation in the field of deep underground engineering. The microseismic multi-parameters (such as the microseismic event count, seismic energy, apparent volume, energy index, apparent stress, and their cumulative values) exhibit unique evolution trends and characteristics prior to the occurrence of a rockburst (Srinivasan et al. 1999; Dou et al. 2018; Liu et al. 2017b; Feng et al. 2015; Ma et al. 2020). Some of the characteristics include strong microseismic activity in rockburst areas, a large amount of energy released due to microseismicity, significant increase in the cumulative apparent volume, and prolonged decrease in the energy index (Tan et al. 2015; Li et al. 2016; Hu et al. 2017). With the expansion of the rockburst database and the rapid development of machine learning methods, the feasibility, accuracy, and timeliness of rockburst prediction and early warning are expected to be further improved through the time series prediction of the microseismic parameters based on deep learning. This type of prediction will play an important role in ensuring the economic benefits of projects and the safety of construction personnel.

Time series data reflect the state or law of factors varying with time. Time series prediction based on deep learning has been developed and widely employed for trend prediction in the stock market, finance, transportation, and other industries (Polson et al. 2017; Thomas et al. 2018; Hou et al. 2019; Anita et al. 2020; Bashar et al. 2020; Zhang et al. 2020a, b, c, d). Rockburst development in deep underground areas is accompanied by multiple microseismic events over a certain period in an enclosed rock area, and there is an evident abnormal variation law in the time series data of the microseismic parameters prior to the occurrence of a rockburst. The time series prediction of the microseismic parameters involves predicting the future trend and evaluating the rockburst risk by thoroughly learning existing time series rules. Rockburst prediction based on machine/deep learning being rapidly developed (Pu et al. 2019). Zhou et al. (2016) used a stochastic gradient boosting model to analyze five potentially related indicators that can help predict rockbursts. Liang et al. (2020) used ensemble learning methods, such as the random forest (RF), adaptive boosting, gradient boosted decision tree, extreme gradient boosting, and light gradient boosting machine, and selected three microseismic parameters as evaluation indicators for rockburst prediction. Ji et al. (2020) used a combination of SVM and genetic algorithm (GA) to study the roles of microseismic waveform data and microseismic energy data in rockburst risk prediction. Moreover, some basic studies on the use of machine/deep learning for classifying microseismic events, denoising of microseismic waveforms, and arrival-time selection of the s/p waves have contributed to improving the accuracy and efficiency of rockburst prediction. Dong et al. (2016) established a classification model for microseismic and blasting events based on the Fisher classifier, naive Bayes classifier, and logistic regression. Shang et al. (2017) provided an idea for the feature extraction and pattern recognition of rock rupture and blasting signals based on a series of models. Andy et al. (2020) found that a convolutional neural network (CNN) trained on a large amount of microseismic data can effectively detect microseismic events. Jiang et al. (2020) proposed an automatic classification method for microseismic events and explosions using an improved complete ensemble empirical mode decomposition with adaptive noise, singular value decomposition, and k-nearest neighbor algorithm. Pu et al. (2020) compared ten machine learning methods, including SVM, BP neural network, naive Bayes classifier, and RF method, in terms of their performance in identifying microseismic events in underground mining. Zhang et al. (2020a, b, c, d) proposed a denoising method based on a fully convolutional encoder–decoder neural network that simultaneously learns the sparse features in the frequency domain and a mask-related mapping function for signal separation. Based on the residual link nested U-Net network (RLU-Net) and Wasserstein generative adversarial network, Zhang et al. (2020a, b, c, d) realized the automatic collection of microseismic waveforms.

In summary, significant advancements have been made in rockburst prediction and microseismic research based on machine/deep learning models. In particular, rockbursts can be prevented effectively and accurately through short-term prediction in the construction stage. However, this type of prediction is mainly based on an on-site monitoring index that helps predict the grade of current rockburst risk; on the other hand, microseismic research based on machine learning mainly uses signal processing methods such as classification, denoising, and detection (arrival-time picking). To improve timeliness, effectiveness, and accuracy of rockburst prediction and provide early warning, it is necessary to study the time series prediction of microseismic parameters based on deep learning.

To overcome the current problems in microseismic and rockburst studies, we performed a time series prediction of the microseismic parameters based on a deep learning method by proposing univariate, multivariate, and multivariate multi-step prediction models. A large amount of time series data pertaining to different rockburst cases are used to train and test these models, and the rockburst risk is interpreted. In addition, two different methods, namely the long short-term memory network (LSTM) and CNN, are used compare the performance of the prediction models. The results show that our method can accurately predict the evolution of the microseismic multi-parameters from the time series data of the complete rockburst process (including in the precursory stage of the rockburst), thus providing a feasible and effective technical method for the prediction

and early warning of rockbursts in deep-buried tunnel engineering applications.

## 2 Time Series Prediction Model of Microseismic Multi-parameter

### 2.1 Methodology

Generally, a complete rockburst can be broadly divided into three stages, including rockburst incubation stage, development stage, and rockburst stage. The multiple parameters associated with microseismic events in each stage have their own performances (Li et al. 2016; Liu et al. 2019; Xue et al. 2020). Figure 1 shows the evolution of multiple microseismic parameters during a typical rockburst. It can be found that three kinds of rockburst indicators ($f(t)$, $\sum g(t)$, and $h(t)$) or their combinations are conducive to evaluate the rockburst risk and further predict rockburst. For example, the cumulative apparent volume increases rapidly, the energy index decreases largely, and the rockburst probability continues to increase in rockburst development stage, indicating that the fracture of surrounding rock expands and approaches to the failure state of rockburst. This stage contains abundant precursor information related to rockburst hazards, which can be used for rockburst prediction. Moreover, the evolution trend of the microseismic parameters over a period of time contributes to the rockburst prediction and avoids the impact of the parameter outliers on the prediction at some time. Therefore, it is important to ascertain which stage the rockburst belongs, that is, to predict the evolution trend of microseismic parameters. To this end, the different indicators and their combinations require various prediction models, and the time series prediction model for the multiple microseismic parameters is constructed in this study.

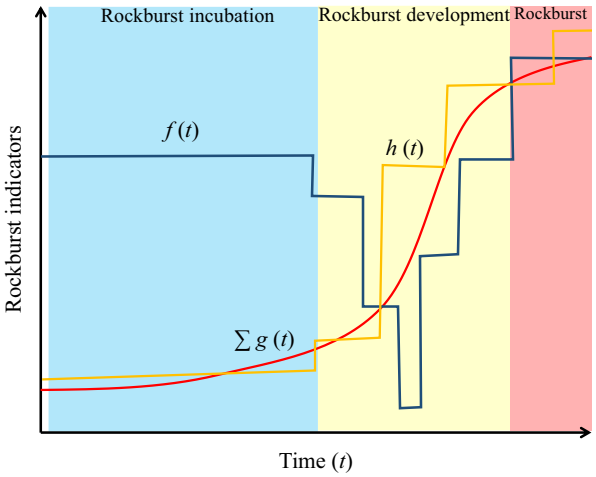


**Fig. 1** Rockburst stage division based on the different indicators. (1) $f(t)$ (blue line) represents the indicator of real-time fluctuations, including energy index, stress drop, apparent stress, etc. (2) $\sum g(t)$ (yellow line) represents the cumulative indicator, including cumulative seismic energy, cumulative apparent volume, cumulative event count, etc. (3) $h(t)$ (red line) represents other indicator constructed from the microseismic parameters, such as rockburst probability

### 2.2 Time Series Prediction Model

#### 2.2.1 Univariate Prediction Model

We call the prediction model for the evolution of the univariate microseismic parameters from time series data as the "univariate prediction model". Figure 2a shows the time series curve of a single variable whose transverse coordinate is calibrated with the equal time distance; the blue and yellow lines indicate the observed and predicted time series, respectively. We need to build a map or model to predict future observations from past observations, and the implementation can be described as follows (see Fig. 2b). *In calculation step 1*, the input time window of the model is the observation sequence of certain time steps (i.e., the length of the time window), and the output is the predicted value of the next time step. Thus, the predicted value is inferred from the observed values. *In calculation step 2*, the input time window is slid forward, and the input to the model should contain the predicted one-step value from the previous calculation step. *In calculation step n*, both the input and output of the model may be predicted values, i.e., the predicted value is inferred from the previous predicted values. The above implementation process requires sliding the input window forward step by step to obtain the prediction curve, which we call the moving-window method.

We need to train the model, e.g., a CNN, that takes a series of past observations as input and outputs the predicted value of the next time step. As such, the sequence of observations must be transformed into multiple examples from which the model can learn. We can divide the sequence into multiple input/output patterns called samples, where certain time steps are used as input, and the next one step is used as the output for the one-step prediction being learned.

Figure 2c shows the architecture of the CNN model. The model input is a 1D vector ($n \times 1$ size) of the observed time series and is followed by a convolutional layer, a max pooling layer, a flattening layer, and a densely connected layer. A padding operation is first performed, and then, the convolution operation expands the depth of the feature while extracting the feature (e.g., the feature expands from 1 layer to $m$ layers, and the feature size becomes $n \times m$). In some cases, the first convolution layer may be followed by a second convolution layer and then connected to the max pooling layer, the task of which is to extract the most significant features from the output of the convolution layer. The feature map is simplified as a 1D vector using the flattening layer between

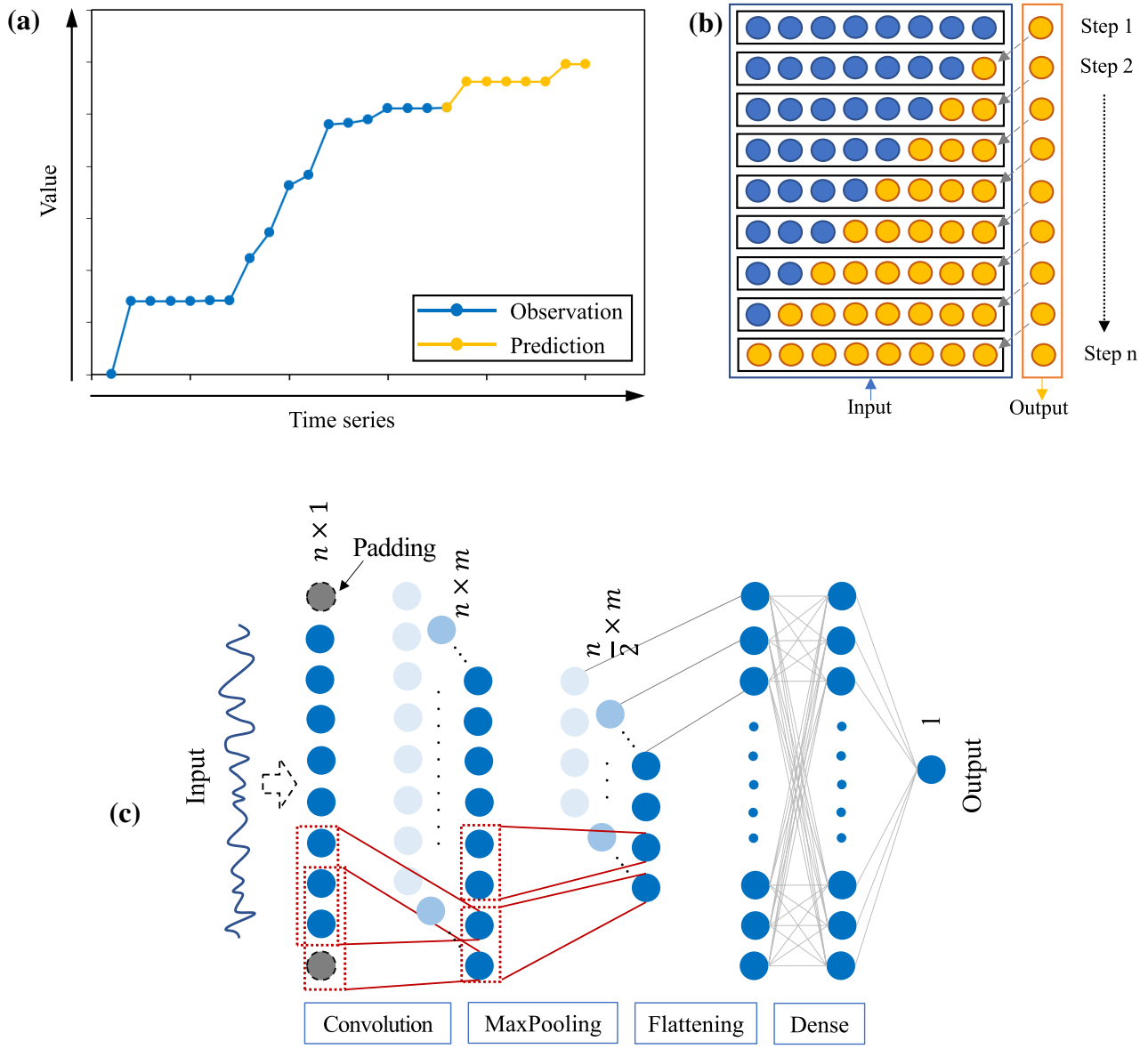


**Fig. 2** Univariate prediction model for microseismic parameters. **a** Time series curve of univariate parameter; **b** implementation of univariate prediction; **c** architecture of the convolution neural network

the max pooling and densely connected layers. Finally, the densely connected layer is used to explain the features and output the one-step prediction.

### 2.2.2 Multivariate Prediction Model

1. *Multiple Parallel Series Model*

   We often analyze rockburst evolution and judge the rockburst risk by combining multiple microseismic parameters (e.g., energy index and cumulative apparent volume) that are typically interrelated. Figure 3a shows the sample curve of the multivariate time series. We need to build a model based on the observations of the multivariate time series to predict the multivariate values of the next time step, which is called the multivariate prediction model of the parallel time series (or multiple parallel series model). Figure 3b illustrates the implementation of the model. *In calculation step 1*, the model input is the observed multivariate sequence (e.g., two variables) with certain time steps, and the output is the multivariate prediction value of the next time step. *In calculation step 2*, the input to the model should contain the multivariate prediction from the previous calculation step. *In calculation step n*, both the input and output of the model can be multivariate predicted values.

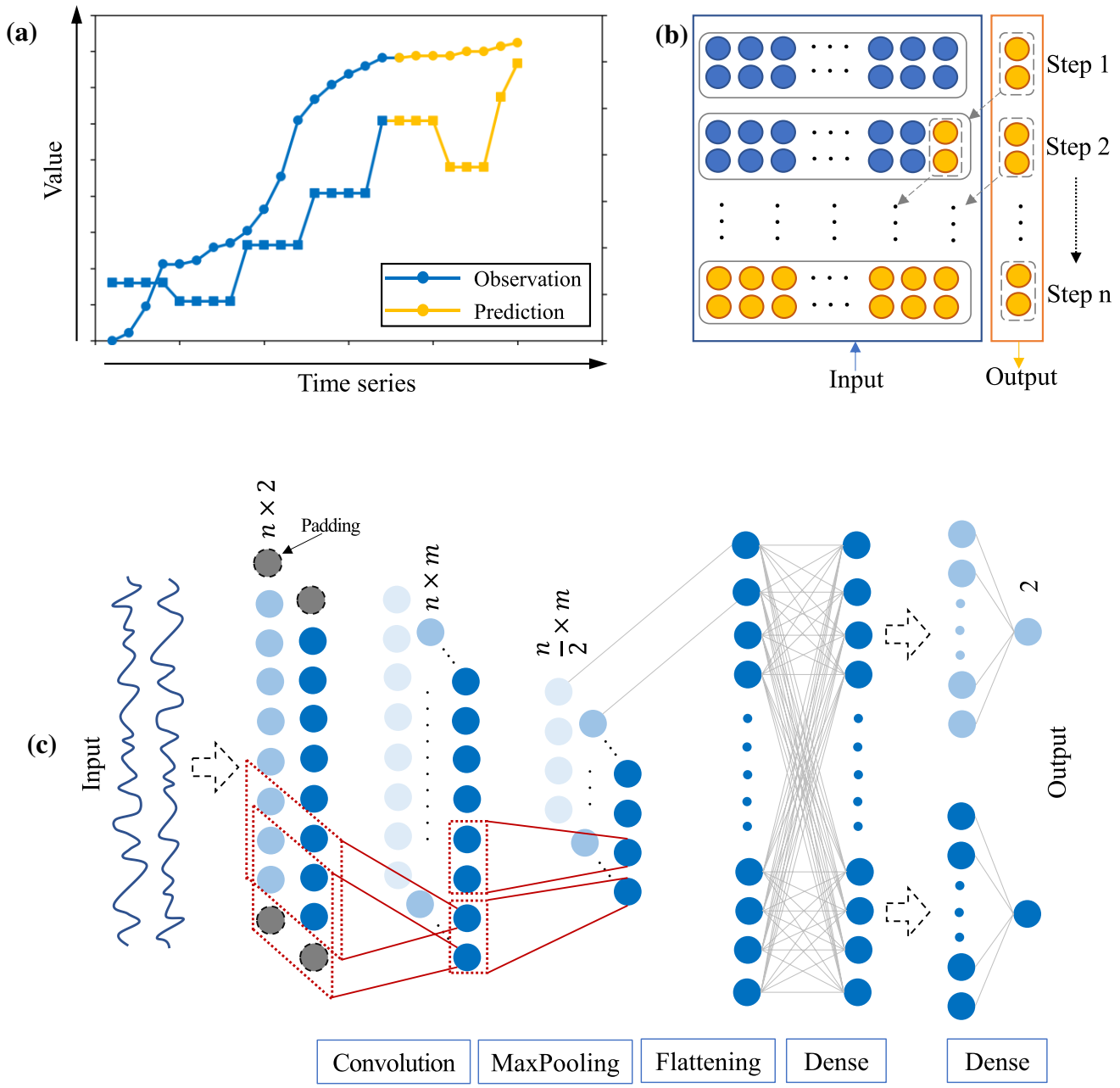


**Fig. 3** Multivariate prediction model for parallel time series. **a** Time series of multivariate parameter; **b** implementation process of prediction; **c** architecture of the convolution neural network

The network structure of the multiple parallel series model is adjusted on the basis of the univariate prediction model (see Fig. 3c). First, the input data dimension (e.g., $n\times2$ represents $n$ time steps and two layers) is put forward for the two time series. At the model output, the features connect multiple independent densely connected layers, i.e., the multivariate prediction values of the next time step are outputted separately. This output strategy may offer more flexibility or better performance depending on the specifics of the problem being modeled. The feature extraction in the middle process of the model is similar to that of the univariate prediction model.

2. *Multiple Input Series Model*

In judging the evolution of a rockburst, it is sometimes necessary to predict the evolution of a new variable based on the existing multivariable observation sequence. We call this the multiple input series prediction model. The new variable and existing multiple variables satisfy certain

functional relationships; for example, a functional relationship can be established between a new variable (rockburst probability) and multiple microseismic parameters (cumulative event number, cumulative seismic energy, and cumulative apparent volume). Figure 4a shows the sample curve of the multivariate input series; the input multivariate time series includes observation and prediction, and the output time series is the prediction of the new variable (indicated by the green line). The implementation process of the prediction model is described in Fig. 4b: *in calculation step 1*, the model input is the observed multivariate sequence with certain time steps (e.g., three variables), and the output is the predicted new variable at the current time step; *in calculation step 2*, the input should contain the one-step prediction of the multiple variables, and the output is the prediction of the new variable; *in calculation step n,* all the inputs may be predicted multivariate values, and the output is also the prediction of the new variable at the current time step.

The network structure of the multivariate input series model is established, as shown in Fig. 4c, after some special considerations. First, the input multivariate sequence is no longer processed by a single convolutional module but by multiple convolutional modules (e.g., three modules), which we call a multi-headed CNN model. This structure may offer more flexibility or better model performance; for example, it allows to configure each module and its parameter settings differently for each input sequence, such as the number of filter maps and the kernel size. After a series of operations of convolution, max pooling, and flattening, the extracted features of the different sequences are concatenated. Finally, the resolution of the feature is reduced by the densely connected layer, and the single-step prediction of the new variable is outputted.

#### 2.2.3 Multivariate Multi-step CNN Model

For the prediction of the above univariate or multivariate time series, the output of the model is the prediction of a single time step; however, some problems may require multi-time step prediction, i.e., a multivariate multi-step prediction model. Figure 5a and b shows the multi-step output of the multivariate time series. *In calculation step 1*, the observed multivariate sequences with certain time steps (e.g., two variables) serve as the model input, and the predicted multivariate values of the next two steps are outputted. *In calculation step 2*, the model input should contain the predicted two-step multivariate values from the previous calculation step. *In calculation step n*, both the input and output of the model may be predicted multivariate values.

Figure 5c shows the network structure of the multivariate multi-step output model, whose input and feature extraction layers are similar to those of the above models. By inputting the parallel time series of the two variables, the feature is extracted and outputted as a $2 \times 2$ matrix after a series of operations in the convolution layer, max pooling layer, flattening layer, and densely connected layer. This output matrix represents the predicted two-step values of the two variables.

## 3 Case Study

### 3.1 Geological Conditions and Microseismic Monitoring System

We performed a time series prediction of multiple microseismic parameters associated with the development of a rockburst in the Micangshan extra-long tunnel of the Sichuan–Shaanxi expressway; this tunnel is the second longest (13.8 km) expressway tunnel in China and the third longest in the world. In the excavation of the K46 + 170 − K45 + 800 mileage section of the tunnel, rockburst hazards due to the high ground stress occurred frequently (Fig. 6). The rockburst areas have the following conditions: the buried depth is in the range of 530–760 m, and the lithology is mainly gabbro and tectonic granulite; the classification of the surrounding rock quality is mainly grade III (medium), indicating a certain number of joints or fissures in the rock mass; the strata of the gabbro and tectonic granulite are interlaced, and multiple rockburst hazards occurred at the section of the tectonic granulite. Based on the identification, the original rock of the tectonic granulite should be gabbro, which undergoes compressive rupture and recrystallizes to form granulite. The rock mass has many microfractures but still has a high residual geo-stress, which is likely to induce rockburst.

Figure 7 shows a microseismic monitoring system and a sensor array layout. Both the tunnels were monitored with three sensors as one group; two sensor groups were distributed at the leading tunnel and one at the following tunnel; three sensors in each group were located at the top and two sides of the tunnel, respectively. The sensor group at the leading tunnel covered the monitoring range of the following tunnel and improved the accuracy of the microseismic source location in this range. A data acquisition station was installed at the lining support area, located in a crossing tunnel between two tubes. The sampling frequency and sampling window were set to 20 kHz and 1.5 s, respectively. The recorded data were collected from 30,000 sampling points with the values in voltage.

To ensure the calculation accuracy of the microseismic parameters, the follow steps were taken: (1) moving invalid sensors to avoid interfering with parameter calculation; (2) distinguishing microseismic data from noise for an effective signal extraction (Zhang et al. 2020a, b, c, d); (3) denoising the microseismic data to obtain clean data (Zhang et al. 2020a, b, c, d); (4) selecting an appropriate index based on

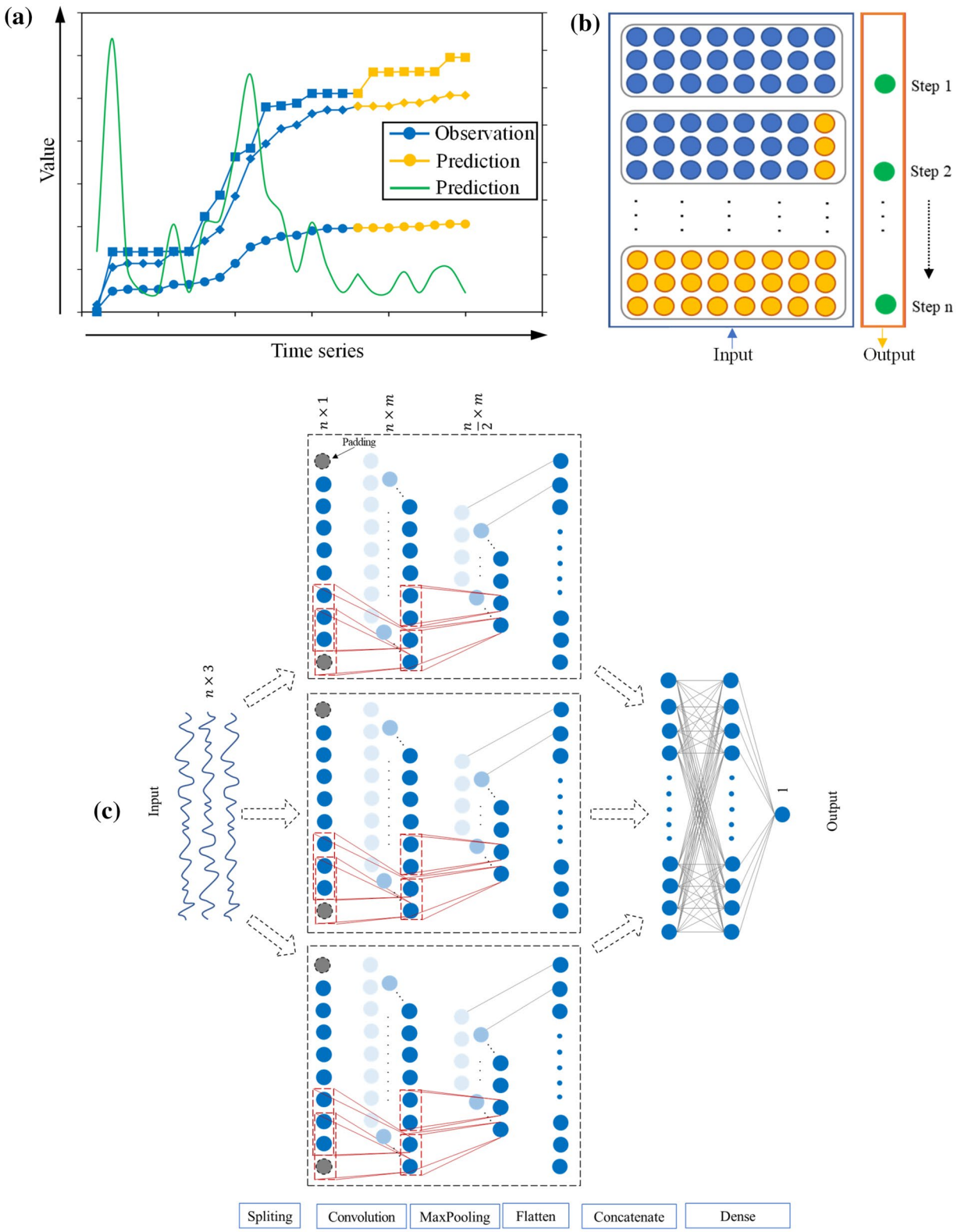


**Fig. 4** Multivariate prediction model for multiple input series. **a** Time series of multivariate parameter; **b** implementation process of prediction; **c** architecture of the convolution neural network

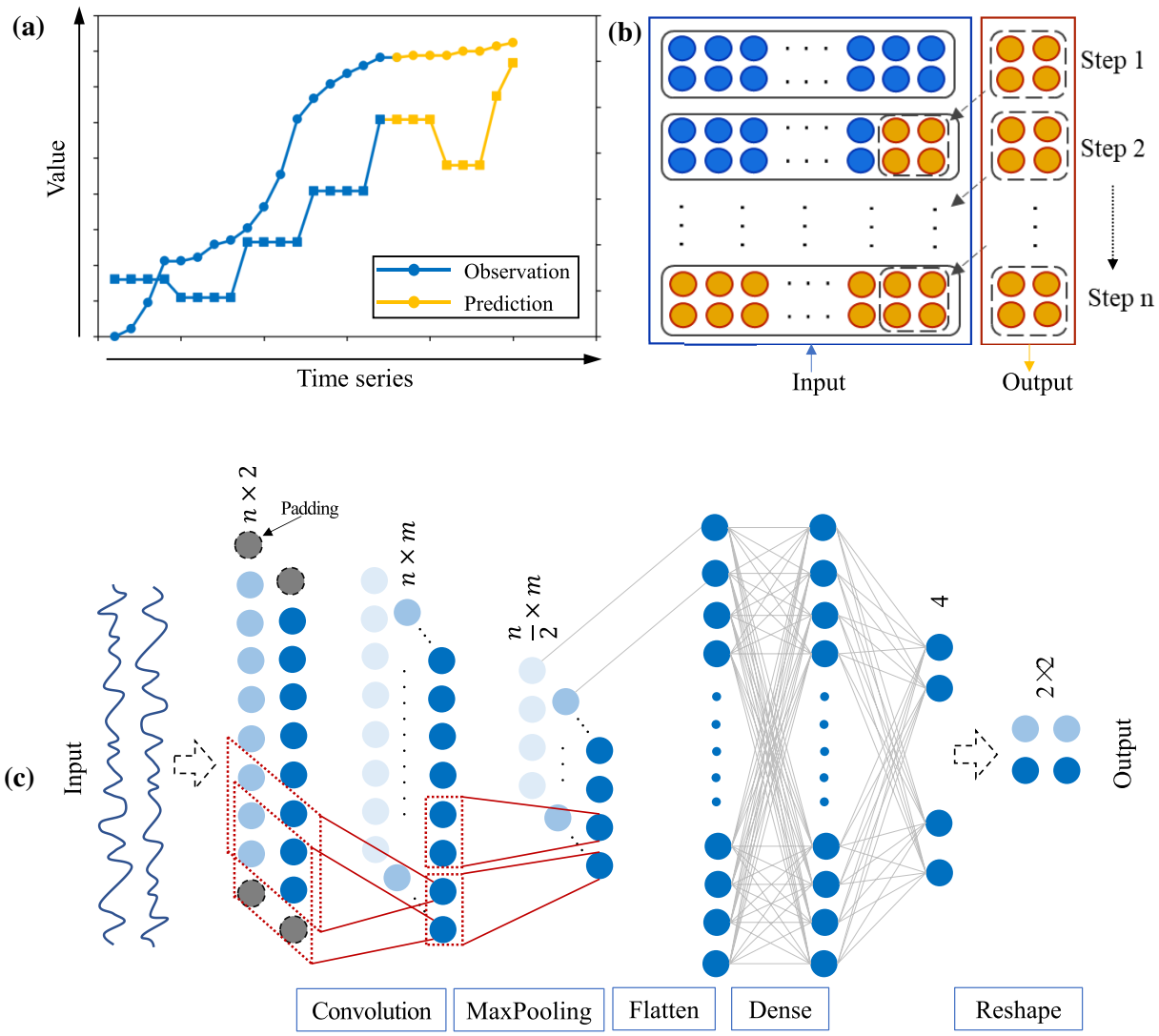


**Fig. 5** Multivariate multi-step prediction model for parallel time series. **a** Time series of multivariate parameter; **b** implementation process of prediction; **c** architecture of the convolution neural network

the geological conditions of tunnel for microseismic parameter calculation. Based on the above steps, the microseismic parameters of the recorded data were processed using a set of standards, ensuring the normalization of the parameter calculation and the accuracy of the subsequent analysis. Table 1 presents the definitions of the microseismic parameters.

### 3.2 Process and Description of Rockbursts

Rockbursts in the Micangshan tunnel originate from the excavation of the tectonic granulite section and often occur on the roof or excavation face of the tunnel. The rockbursts occur with a thunder-like bang and subsequently exhibit a splitting sound; the broken rocks are ejected or they collapse. The rockburst zones are mostly controlled by a dominant structural plane, or present a wedge or fornix shape controlled by two or more structural planes, with a maximum depth of up to 3 m (Fig. 8a). These rockbursts exhibit characteristics such as a high-energy release and a wide influence range. The maximum energy of a microseismic event can reach 1 million joules, which is even comparable to that reported during tunnel blasting. The high energy released affects the tunnel equipment and surrounding rock, resulting in shaking or overturning of the equipment, cracking of the tunnel floor (floor heave), cracking of the tunnel sidewall (sidewall heave), and initial support failure (Fig. 8b). For example, the high energy released from a rockburst may cause cracks at the same mileage in the adjacent tunnel (Fig. 8c).

1. Microseismic Event Count and Seismic Energy

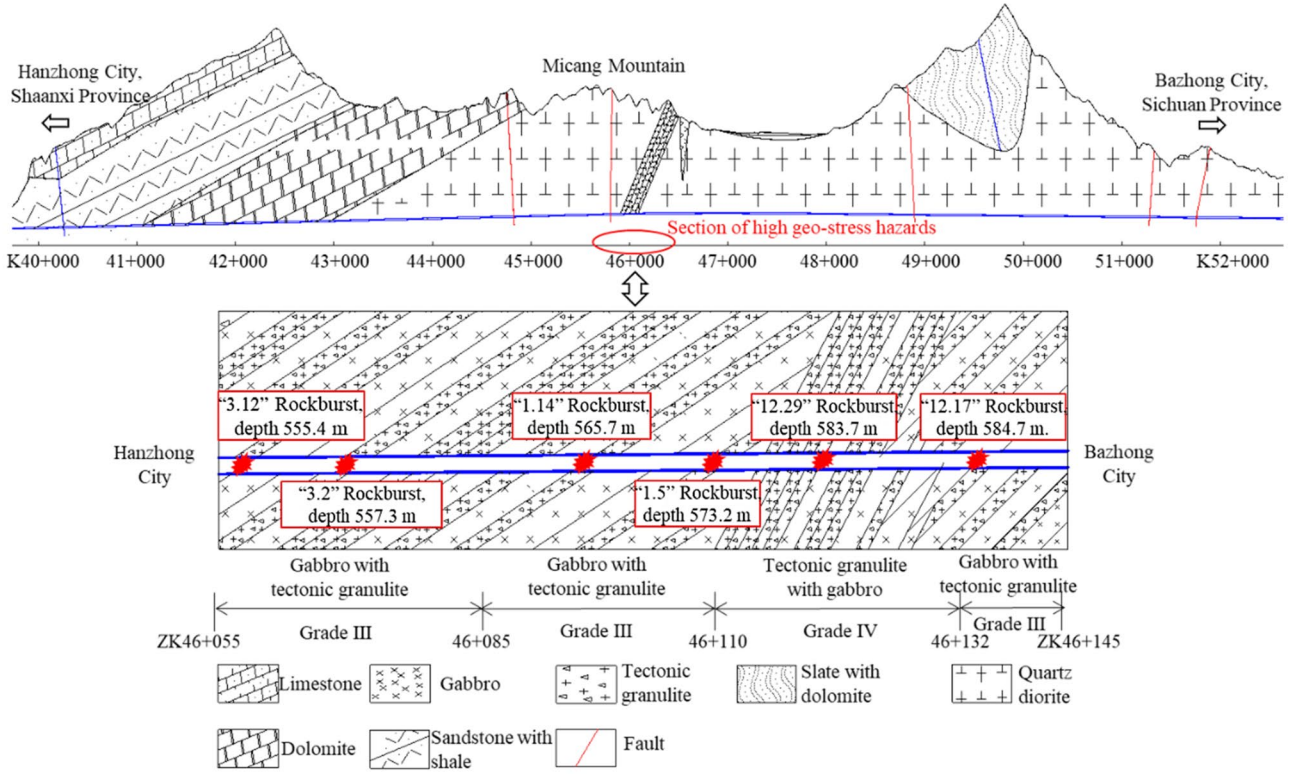


**Fig. 6** Geological cross-section along the Micangshan tunnel, China (Ma et al. 2019)

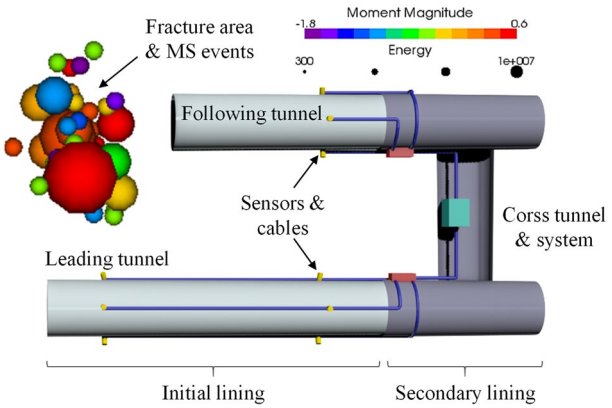


**Fig. 7** Layout of the microseismic monitoring system installed in the Micangshan tunnel

The evolution of the microseismic parameters during rockburst is significant. Figure 9 shows the variations in the daily microseismic event count and microseismic activity index (S value, proposed by Liu et al. 2018) during a typical rockburst. The activity and frequency of the microseismic events before the rockburst are high, and the overall trend is gradually rising (except for the "1.14" rockburst, where the trend first increases and then decreases). The microseismic event count and S value are still high on the day of the rockburst; however, both decrease significantly after the rockburst.

Microseismic events can be classified into three categories based on the amount of energy released: a low-energy event ($\leq 10^4$ J), a medium-energy event ($10^4$–$10^5$ J), and a high-energy event ($\geq 10^5$ J). Figure 10 shows that the daily cumulative energy and medium- and high-energy incidences of the microseismic events reach maximum in 1–2 days before the rockburst. They remain high on the day of the rockburst but decrease significantly thereafter.

2. Energy Index and Cumulative Apparent Volume

Figure 11 shows the evolution of the energy index and cumulative apparent volume during representative rockbursts. The energy index fluctuates, and the cumulative apparent volume continues to increase. The closer the occurrence of rockburst, the lower the energy index is in the oscillation, and the cumulative apparent volume increases sharply. Notably, this precursor characteristic of rockburst development also appears during the strong stress adjustment activity after tunnel blasting; however, in this case, the energy index curve recovers quickly and exhibits a significant fluctuation.

3. Rockburst Probability

**Table 1** Definitions of microseismic parameters (Zhao et al. 2018; Dai et al. 2017; Liu et al. 2018)

| Parameter name | Definition | Description |
|---|---|---|
| Seismic energy | $E = 8/5\pi\rho vR^2 \int_0^{t_s} U_{corr}^2(t)dt$ | $E$ represents the Elastic strain energy released by rock mass fracture. $\rho$ is the rock density, $V$ is the microseismic wave velocity, and $R$ is the distance from the sensor to the source. $t_s$ is the time span of the seismic wave signal. $U_{corr}$ is the displacement function of the seismic wave, that is, the velocity pulse time function |
| Apparent volume | $V_A = \frac{M_0^2}{2\mu E} = \frac{M_0}{2\sigma_a}$ | The apparent volume $V_A$ is the volume of the rock mass in the inelastic deformation area of the microseismic source ($m^3$). $\mu$ is shear modulus, $E$ is seismic energy, $M_0$ is seismic moment, and $\sigma_a$ is the apparent stress |
| Energy index | $EI = \frac{E}{\overline{E}} = 10^{-c}\frac{E}{M_0^d}$ | EI is the ratio of instantaneous energy to average energy. $E$ is the seismic energy, and $M_0$ is the seismic moment. $c$ and $d$ are the linear slope and intercept fitted by $LgM_0$ and $LgE$ |

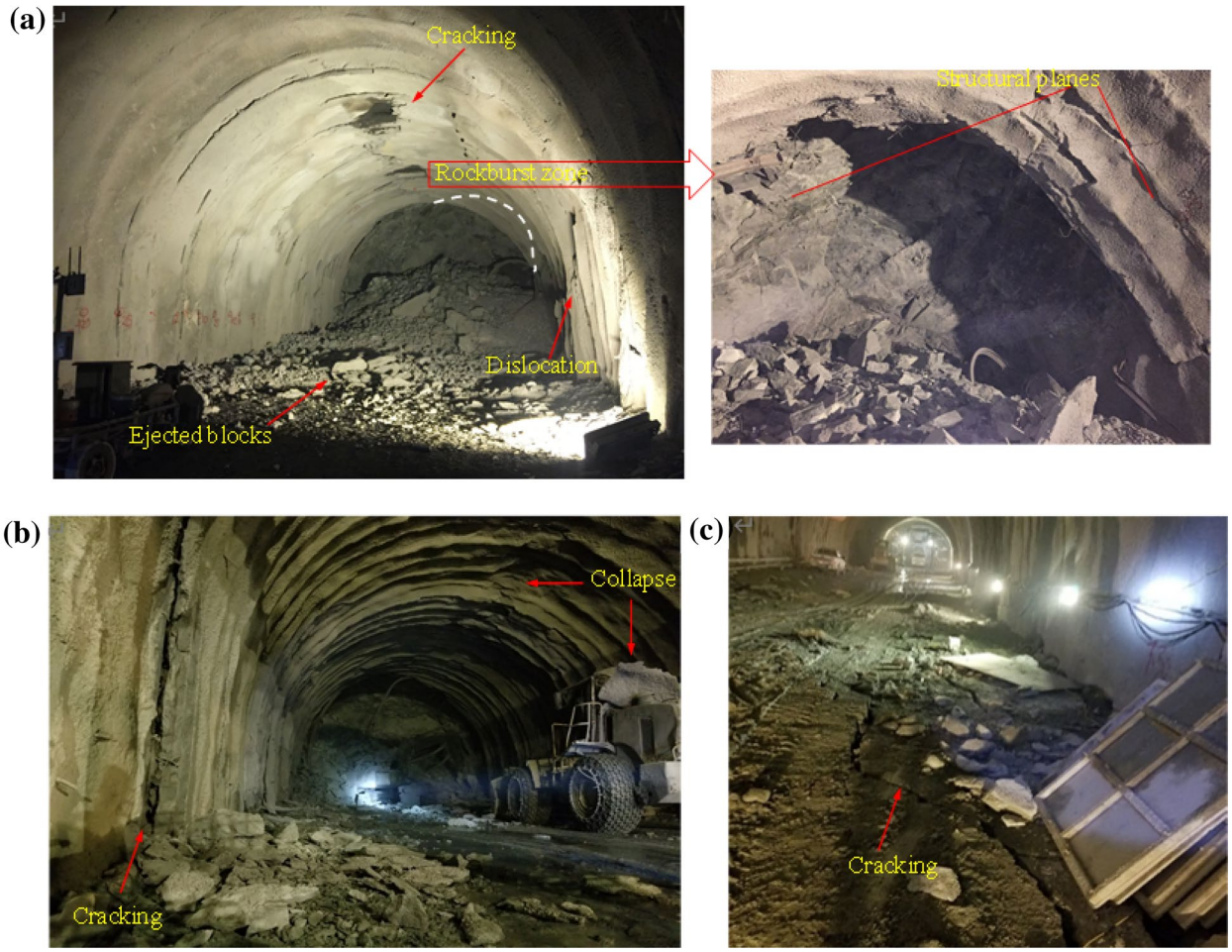


**Fig. 8** Rockburst and damage characteristics of the Micangshan tunnel

We establish an evaluation index of the rockburst probability using the similarity measure method, which is based on three parameters: the microseismic event count, seismic energy, and apparent volume (referring to the Chinese technical specification for rockburst risk assessment in hydropower engineering). The similarity measure (or distance measure) method involves measuring the relationship between different objects in the mining of time series data. The Euclidean distance is the most widely used similarity measure method. The Euclidean distance $D$ between data points $A$ and $B$ can be defined as

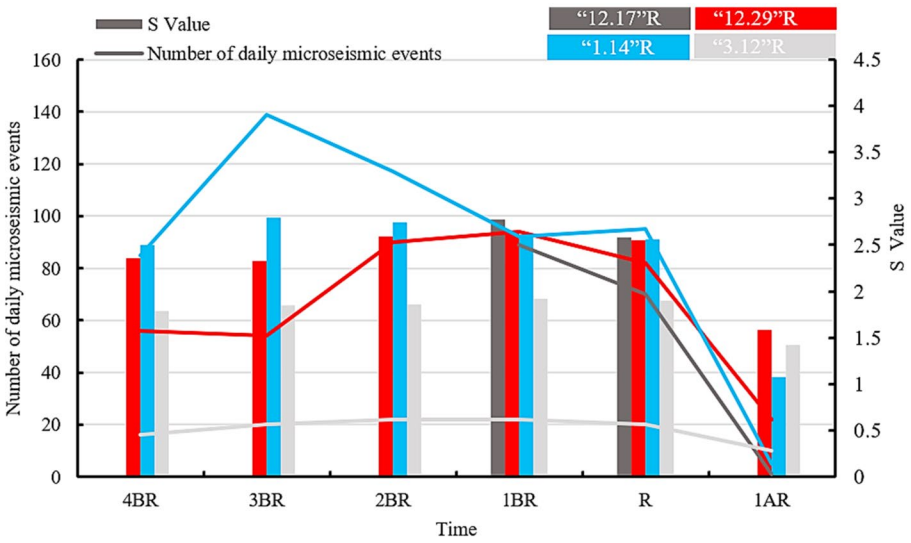


**Fig. 9** Number of daily microseismic events and S value before and after rockburst occurrence. The processes of four typical rockbursts, namely "12.17," "12.29," "1.14," and "3.12," are illustrated. "4BR" denotes 4 days before the rockburst; "R" denotes the day of rockburst occurrence; "1AR" denotes 1 day after rockburst

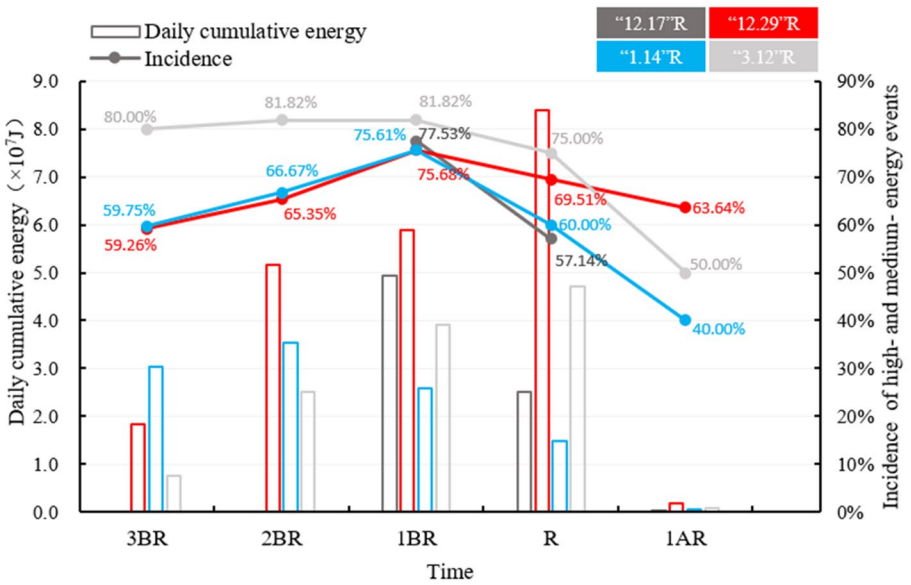


**Fig. 10** Daily cumulative seismic energy and incidences of high- and medium-energy events during the rockburst process

$$D(A,B) = \sqrt{\sum_{i=1}^{n} (a_i - b_i)^2}. \quad (1)$$

Here, $n$ denotes the number of components of the data point; where $n$ equals 3, which refers to the above three microseismic parameters. Because the microseismic event count, seismic energy, and apparent volume have different dimensions, it is better to normalize the three parameters and ensure that their values are distributed between 0 and 1. Subsequently, each Euclidean distance between the parameter values in the rockburst development process and that at the rockburst occurrence is calculated; the result is also distributed between 0 and 1. The lower the value, the higher the similarity between the microseismic parameters at the current time and that at rockburst occurrence, and the greater the possibility of a rockburst. Therefore, the probability of rockburst occurrence is defined as (1-normalized Euclidean distance) × 100%, i.e., the probability at the rockburst occurrence time is 100%. Figure 12 shows the probability evolution of the "1.5" rockburst in the Micangshan tunnel. The rockburst probability fluctuates and increases continuously to 1.0 (i.e., 100%).

### 3.3 Training and Testing of Time Series Prediction Model

1. Model Construction and Training

Because the index magnitude of the cumulative event number, cumulative seismic energy, and cumula-

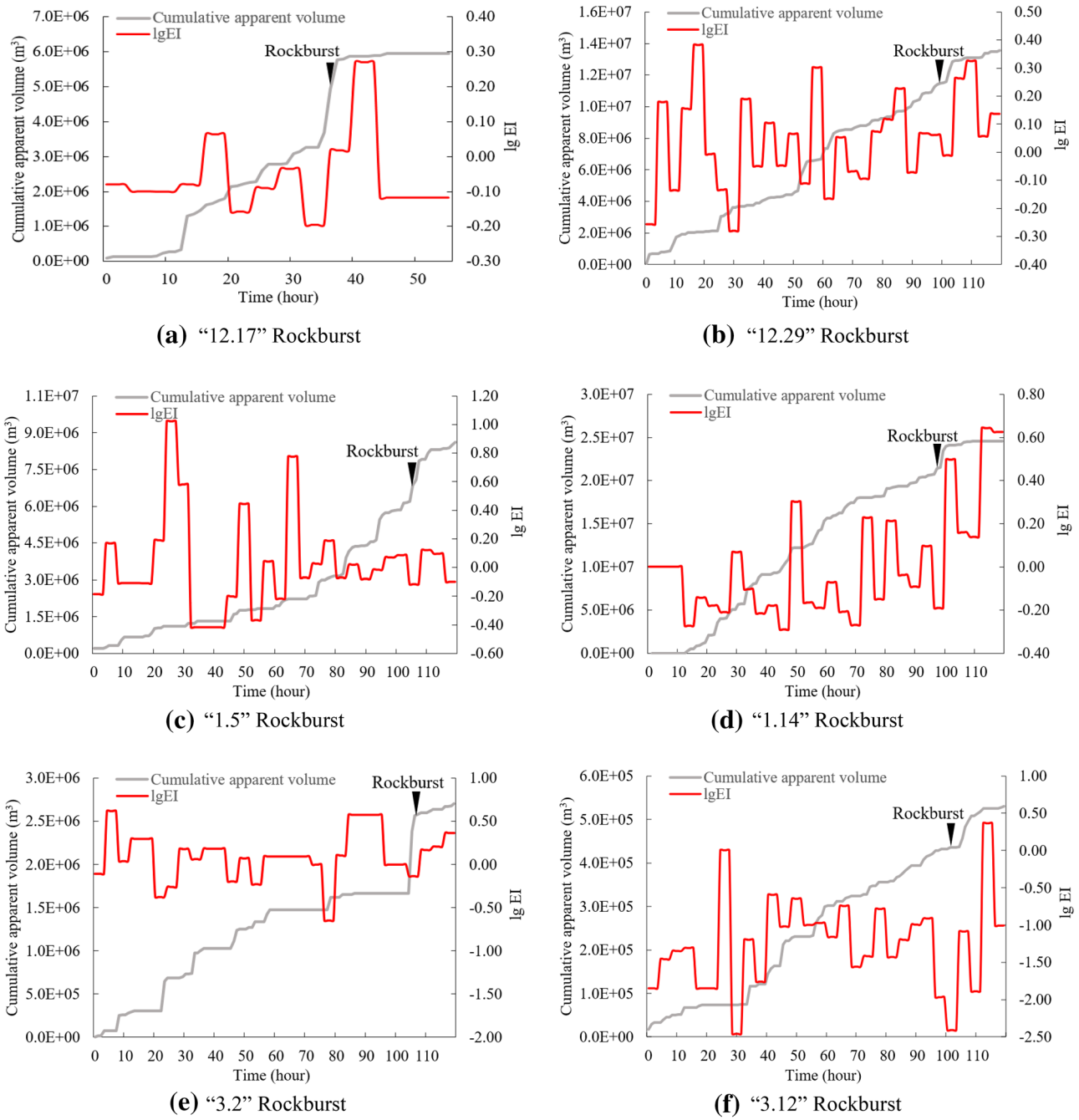


**Fig. 11** Time series of cumulative apparent volume and energy index during rockbursts

tive apparent volume are not uniform (ranging from $10^2$ to $10^8$), it is necessary to standardize the data before model training. The following formula is used to scale the index value between 0 and 1:

$$\overline{X} = \log_{10}^{X} / 10. \tag{2}$$

Here, $X$ denotes the adopted microseismic parameters. Standardization can not only reduce the numerical difference but also accelerate the convergence of the model. Moreover, the original value can be easily recovered by anti-standardization. Figure 13 shows the image before and after the data standardization of a complete rockburst in the Micangshan tunnel (taking the cumulative event number, cumulative energy, and cumulative apparent volume as examples).

Through the data preprocessing (standardization and isochronization), the time series curves of the micro-

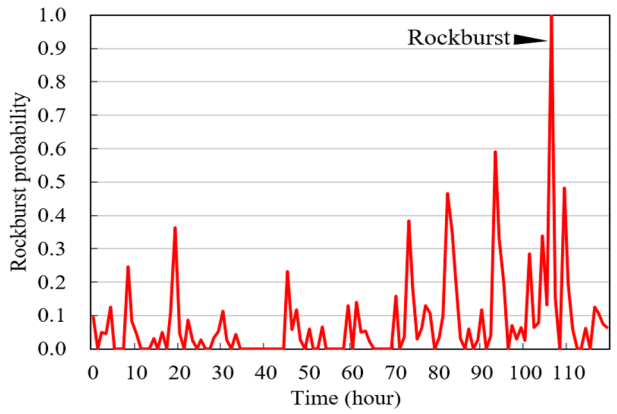


**Fig. 12** Rockburst probability evolution during "1.5" rockburst

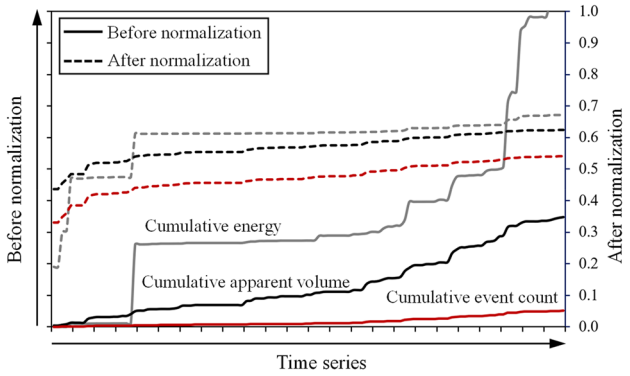


**Fig. 13** Data image before and after processing of rockburst

seismic multi-parameters were established, and the following sample databases were established for model training:

i. The database of the cumulative event number, cumulative apparent volume, and cumulative energy was established for training the univariate prediction model.
ii. The database was established on the basis of the cumulative event number, cumulative energy, cumulative apparent volume, and rockburst probability. It is mainly used for training the multiple input series model, i.e., the inputs are multiple sequences of the cumulative event number, cumulative energy, and cumulative apparent volume, and the output is the constructed rockburst probability.
iii. The database was constructed with the cumulative apparent volume and energy index for training the multiple parallel series model (including the single-step and multi-step output models), i.e., the input is the parallel time series of the cumulative apparent volume and energy index, and the output is the single-step or multi-step predictive values of these two variables.

The data pertaining to the "12.29," "1.5," "1.14," "3.2," and "3.12" rockbursts were used to construct a database for model training, which is different from general database integration construction. The data of these rockbursts were randomly selected and inputted to the model for training in a successive manner; that is, after completing the training with one set of rockburst data, the model was trained with the next set of rockburst data.

In the model training, the selected length of the time window (time steps) for the input sample will affect the training result. When the time window is set too small, it is difficult for the model to learn the features of the microseismic parameters in the time dimension, and when the time window is too large, it may contain too many features of the time dimension, thereby affecting the prediction performance of the model. Therefore, a suitable time window length can make the model obtain a good fitting effect (Song et al. 2017; Wollmer et al. 2010). Through a comprehensive consideration, the input length of the time window is set to 12 for the training model. Thus, the input sample dimensions of the univariate prediction model, multiple input series model, multiple parallel series model, and multivariate multi-step prediction model are 12×1, 12×3, 12×2, and 12×2, respectively, where the first number (i.e., 12) is the length of the time window and the second number is the channel. The Batch size is set to 16 in the process of model training; the learning rate is set to 0.001 considering the prediction effect and training speed; the activation functions are set to Elu and Sigmoid; the loss function is selected as the MSE, and it is optimized using the Adam algorithm. Moreover, the Earlystopping operation is used to avoid over-fitting during model training. Table 2 presents the structure and parameter setting of the established prediction models.

2. Testing of Univariate Prediction Model

We test the data pertaining to the "12.17" rockburst, which was not involved in the training. The test was implemented on the basis of the observation data of the complete rockburst process, i.e., all the input samples are from the observation sequence and do not include the predicted value of the model output. The indicators (Table 3) are used to evaluate the test results of each model. The MAE and RMSE are indicators used to evaluate the error between the prediction and the observation; MAPE not only considers the error between the prediction and the observation but also considers the ratio of the error to the true value, which is a relative value; $R^2$ is in the range of 0–1, and the closer the value is to 1, the closer the predicted value of the model is to the true value.

Figure 14 shows the test results of the univariate prediction model; the yellow line represents the observation

**Table 2** Structure and parameter setting of different prediction models

| Univariate prediction model | | | | Multivariate prediction model of multiple input series | | | | | | Multivariate prediction model of parallel time series | | | | Multivariate multi-step prediction model | | | |
|---|---|---|---|---|---|---|---|---|---|---|---|---|---|---|---|---|---|
| L | O | K/S | AF | L | O | | | K/S | AF | L | O | K/S | AF | L | O | K/S | AF |
| | | | | | #1 | #2 | #3 | | | | | | | | | | |
| CNN 1 | 12×64 | 2/1 | Elu | CNN 1 | 12×64 | 12×64 | 12×64 | 2/1 | Elu | CNN 1 | 12×64 | 2/1 | Elu | CNN 1 | 12×64 | 2/1 | Elu |
| CNN 2 | 12×128 | 2/1 | Elu | CNN 2 | 12×64 | 12×64 | 12×64 | 2/1 | Elu | CNN 2 | 12×128 | 2/1 | Elu | CNN 2 | 12×128 | 2/1 | Elu |
| Pool 1 | 6×128 | 2/2 | | Pool 1 | 6×64 | 6×64 | 6×64 | 2/2 | | Pool 1 | 6×128 | 2/2 | | Pool 1 | 6×128 | 2/2 | |
| CNN 3 | 6×128 | 2/1 | Elu | CNN 3 | 6×128 | 6×128 | 6×128 | 2/1 | Elu | CNN 3 | 6×128 | 2/1 | Elu | CNN 3 | 6×128 | 2/1 | Elu |
| CNN 4 | 6×256 | 2/1 | Elu | CNN 4 | 6×128 | 6×128 | 6×128 | 2/1 | Elu | CNN 4 | 6×256 | 2/1 | Elu | CNN 4 | 6×256 | 2/1 | Elu |
| Pool 2 | 3×256 | 2/2 | | Pool 2 | 3×128 | 3×128 | 3×128 | 2/2 | | Pool 2 | 3×256 | 2/2 | | Pool 2 | 3×256 | 2/2 | |
| CNN 5 | 3×256 | 2/1 | Elu | CNN 5 | 3×256 | 3×256 | 3×256 | 2/1 | Elu | CNN 5 | 3×256 | 2/1 | Elu | CNN 5 | 3×256 | 2/1 | Elu |
| CNN 6 | 3×256 | 2/1 | Elu | CNN 6 | 3×256 | 3×256 | 3×256 | 2/1 | Elu | CNN 6 | 3×256 | 2/1 | Elu | CNN 6 | 3×256 | 2/1 | Elu |
| Pool 3 | 1×256 | 2/2 | | Pool 3 | 1×256 | 1×256 | 1×256 | 2/2 | | Pool 3 | 1×256 | 2/2 | | Pool 3 | 1×256 | 2/2 | |
| Flaten | 256 | | | Flaten | 256 | 256 | 256 | | | Flaten | 256 | | | Flaten | 256 | | |
| Dense 1 | 64 | | Sigmoid | Concatenate | 768 | | | | | Dense 1 | 64 | | Elu | Dense 1 | 64 | | Elu |
| Dense 2 | 1 | | Sigmoid | Dense 1 | 64 | | | | Elu | Dense 2–1 | 1 | | Elu | Dense 2 | 4 | | Elu |
| | | | | Dense 2 | 1 | | | | Elu | Dense 2–2 | 1 | | Elu | | | | |

L represents the neural layer, O represents the output size of the layer, K/S represents the kernel size and stride, AF represents the activation function; CNN represents the convolutional neural layer, Pool represents the max pooling layer, Flatten represents the flattening operation, and dense represents the dense layer

**Table 3** Evaluation indicators of model performance

| Indicator name | Definition | Description |
|---|---|---|
| Mean absolute error, *MAE* | $MAE = \frac{1}{n}\sum_{i=1}^{n}\lvert y_i - \overline{y_i}\rvert$ | $y_i$ and $\overline{y_i}$ are the observed and predicted values, respectively, and the n is the sample size of the data. The index represents the average absolute error of the predicted and observed values |
| Root-mean-square error, *RMSE* | $RMSE = \sqrt{\frac{1}{n}\sum_{i=1}^{n}(y_i - \overline{y_i})^2}$ | This index represents the root mean square error of the predicted and observed values of all samples |
| Mean absolute percent error, *MAPE* | $MAPE = \sum_{i=1}^{n}\left\lvert\frac{y_i - \overline{y_i}}{y_i}\right\rvert \times \frac{100}{n}$ | This indicator represents the percentage of errors between predicted and observed values |
| Coefficient of determination, $\boldsymbol{R^2}$ | $R^2 = 1 - \frac{\sum_{i=1}^{n}(y_i - \overline{y_i})^2}{\sum_{i=1}^{n}(y_i - mean(y))^2}$ | *mean* represents the average of the observed values; the closer the index value is to 1, the better the prediction performance of the model |

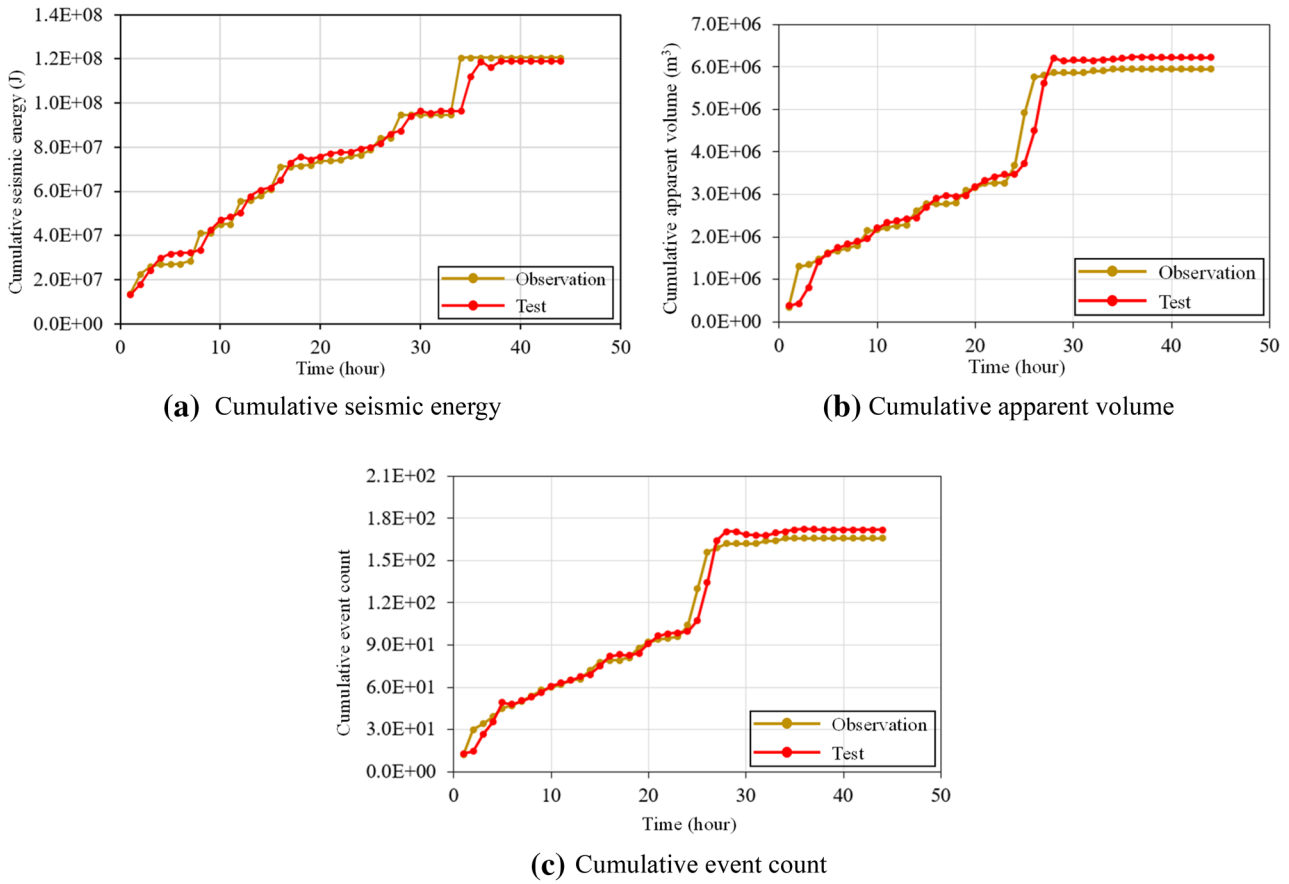


**(a)** Cumulative seismic energy

**(b)** Cumulative apparent volume

**(c)** Cumulative event count

**Fig. 14** Test results of the univariate prediction model

curve, and the red line represents the test curve obtained based on the observation curve as the input sample. The fitting between the observed and predicted values of the cumulative energy, cumulative apparent volume, and cumulative event number is good. Because of the large dimensional difference between each microseismic parameter, the determination coefficient $R^2$ is selected to evaluate the model performance quantitatively. The $R^2$ values of the univariate prediction model for the cumulative energy, cumulative apparent volume, and cumulative event number are 0.978, 0.962, and 0.982, respectively, indicating that the test performance of the model is ideal.

3. Testing of Multiple Input Series Model

Figure 15 shows the test results obtained using the multiple input series model. The test curve of the rock-

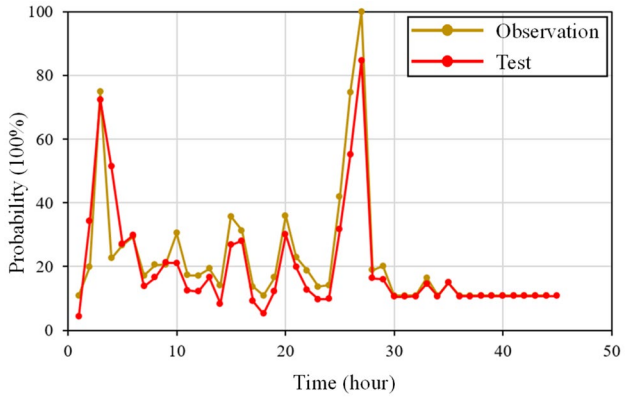


**Fig. 15** Test result of multiple input series model

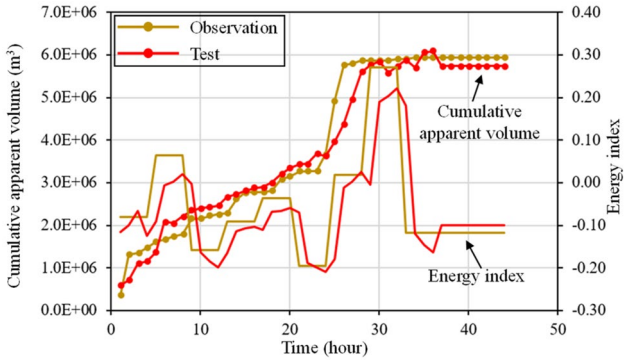


**Fig. 17** Test result of the multivariate multi-step prediction model

burst probability is obtained on the basis of the time series of the cumulative energy, cumulative apparent volume, and cumulative event number as input samples. The fitting between the true and test values is good, and the $R^2$ coefficient is 0.847, which also proves the good prediction performance of the model.

4. Testing of Multiple Parallel Series Model

Figure 16 shows the test results of the multiple parallel sequence models. Clearly, the fitting between the observation and test curves of the cumulative apparent volume is good, and the $R^2$ coefficient is 0.968. The fitting between the observed and predicted values of the energy index is moderate, and the $R^2$ coefficient is only 0.684, which may be due to the large fluctuation in the energy index curve. However, the test curve of the energy index is consistent with the trend in the observation curve, indicating that the multiple parallel series model can yield an accurate prediction.

5. Testing of Multivariate Multi-step Prediction Model

Figure 17 shows the test results of the multivariate multi-step output model. The fitting between the observed and predicted values of the cumulative apparent volume and energy index is worse than that of the multiple parallel series model, and the determination coefficient $R^2$ is also reduced to 0.910 and 0.617, respectively. Therefore, the prediction performance of the multi-step output model is lower than that of the single-step output model.

6. Robustness Test of Time Series Prediction Models

To further test the performance of the time series prediction models, the disturbances were introduced in the data to evaluate the robustness and stability of the models. The red line in Figure 18 represents the test curve based on the observation curve corresponding to the disturbances as the input (blue dotted line). The models have a good time series prediction performance, even when the observed data contain disturbances. Moreover, there is a good fitting between the observation and test curves of the cumulative energy, cumulative apparent volume, cumulative event number, and rockburst probability, with their $R^2$ values being 0.974, 0.959, 0.979, and 0.801, respectively. This demonstrates the robustness and stability of the univariate prediction model and multiple input series model. For the multiple parallel series model and multivariate multi-step prediction model, the observation and test curves of the cumulative apparent volume have a good fit, with $R^2$ values of 0.945 and 0.939, respectively. However, the fitting of the energy index is not ideal, with $R^2$ values of 0.454 and 0.437, respectively. Nevertheless, the trend in test curve of the energy index is consistent with the observation curve trend, which is similar to the test results of the observations (Figures 16 and 17). Therefore, the time series prediction models have good stability and robustness under the influence of disturbances.

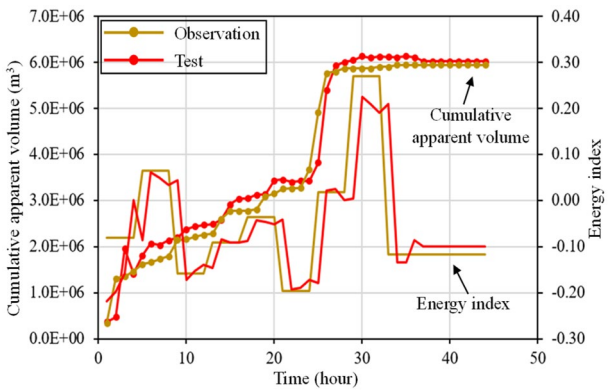


**Fig. 16** Test result of multiple parallel series model

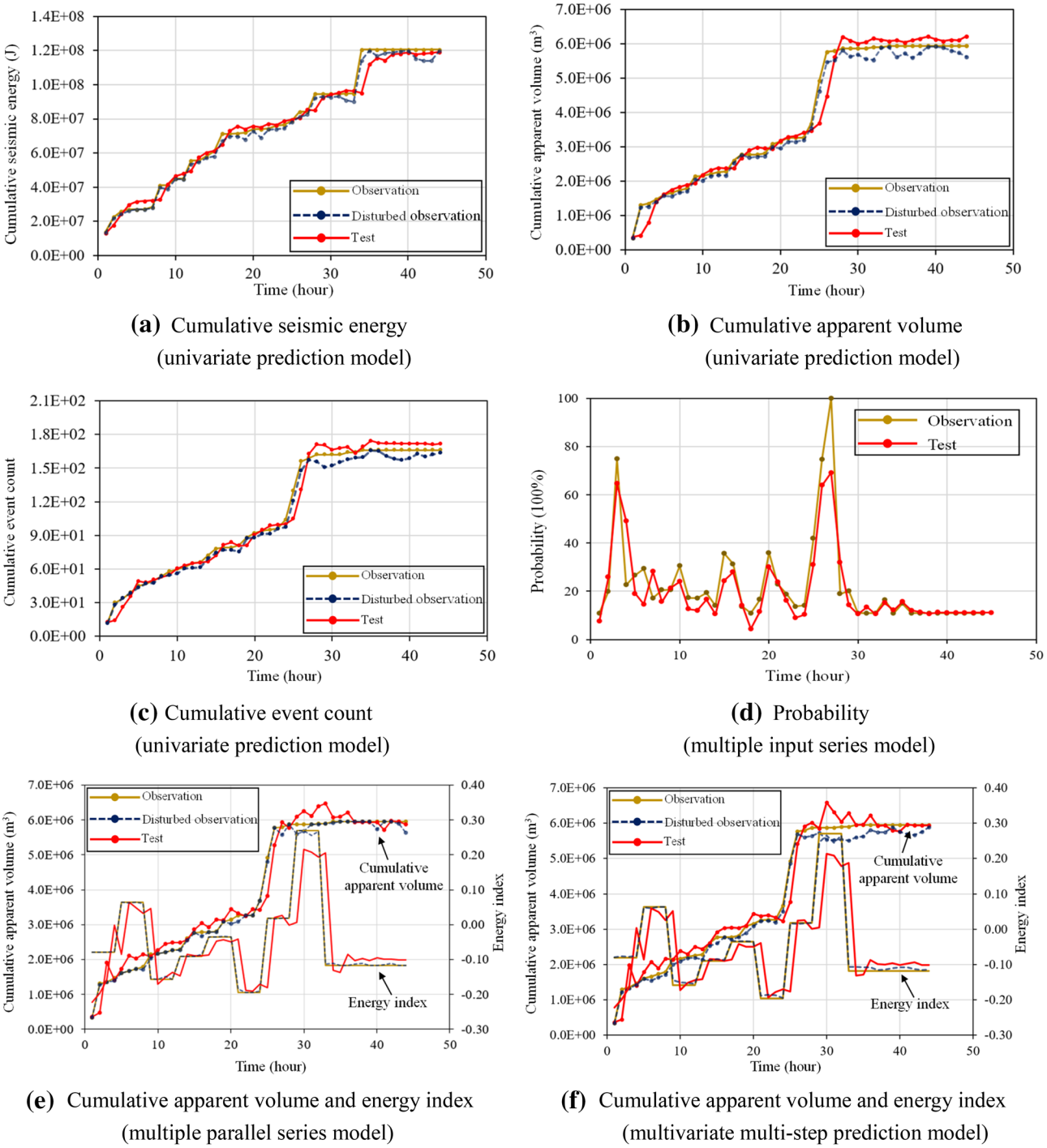


**(a)** Cumulative seismic energy (univariate prediction model)

**(b)** Cumulative apparent volume (univariate prediction model)

**(c)** Cumulative event count (univariate prediction model)

**(d)** Probability (multiple input series model)

**(e)** Cumulative apparent volume and energy index (multiple parallel series model)

**(f)** Cumulative apparent volume and energy index (multivariate multi-step prediction model)

**Fig. 18** Test result of the robustness of time series prediction models

## 4 Discussion

### 4.1 Comparative Studies

The classical LSTM is selected to compare and verify the result of the time series prediction models of the microseismic multi-parameters. The LSTM model has significant advantages in time series modeling owing to its unique structural characteristics, comprising an input gate, an output gate, and a forgetting gate, as well as a memory unit. A three-layer LSTM network structure was adopted in this study. The numbers of hidden units in the first, second, and third layers were 64, 128, and 256, respectively. Before the comparative analysis, the parameters

and structure of the two networks were adjusted, and the optimal performance was achieved.

1. Comparison of Univariate Prediction Model

   Figure 19 shows the test curve of the univariate prediction model based on the two networks for a complete rockburst process. The MAE, RMSE, MAPE, and $R^2$ evaluation indices of the model are recorded in Table 4. The $R^2$ coefficients of the LSTM and CNN models are greater than 0.96 for the accumulative energy and accumulative apparent volume, indicating a good fit between the observation and test curves; the performance of the LSTM model is slightly better as the MAE, RMSE, and MAPE indicators decrease. The test performance of the CNN model is slightly better for the cumulative event number, and its MAE, RMSE, and MAPE indices are reduced by 6.6%, 6.6%, and 10.5%, respectively, compared with that of the LSTM model. In summary, both the LSTM and CNN models can achieve good univariate prediction results.
2. Comparison of Multiple Input Series Model

   Figure 20 shows the test curve generated by the multiple input series prediction model based on the two networks, and the evaluation results in terms of the MAE, RMSE, MAPE, and $R^2$ are recorded in Table 3. The CNN model performs slightly better than the LSTM model for the constructed index of the rockburst probability. The $R^2$ coefficient of 0.847 indicates that the observed values fit better with the test values; the MAE, RMSE, and MAPE indices are reduced by 28.3%, 20.9%, and 36.2%, respectively, indicating that the multiple input series model based on the CNN is more suitable for predicting the constructed index of the rockburst probability.
3. Comparison of Multiple Parallel Series Model

   Figure 21 shows the test curve generated by the multiple parallel series model based on the two networks. The test results of the CNN and LSTM models for the cumulative apparent volume are good; the CNN slightly outperforms the LSTM model, the $R^2$ coefficient is higher, and the MAE, RMSE, and MAPE indices are reduced. The performance

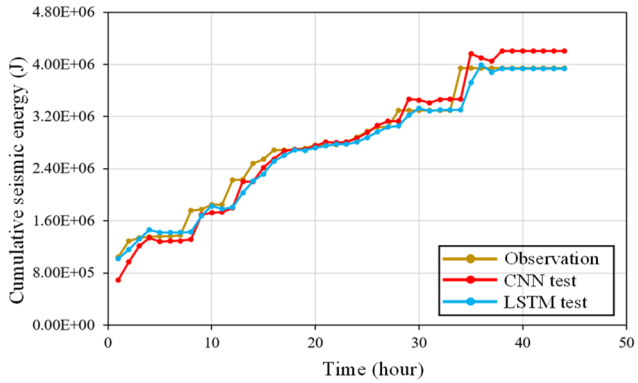


**(a)** Cumulative seismic energy

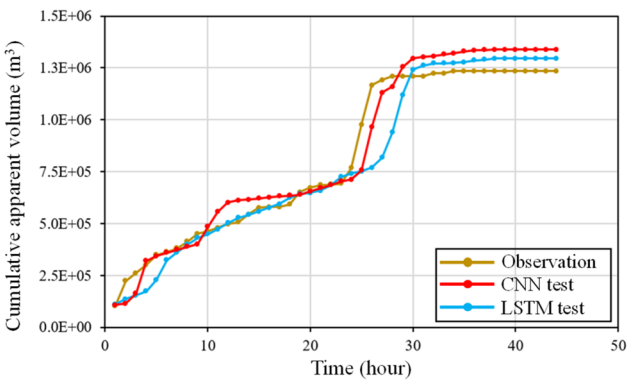


**(b)** Cumulative apparent volume

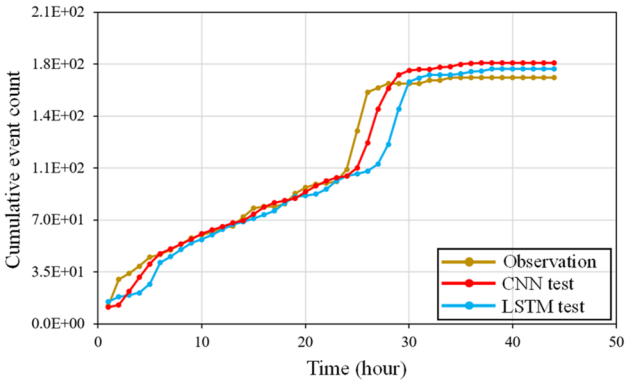


**(c)** Cumulative event count

**Fig. 19** Comparison of univariate prediction results with CNN and LSTM networks

**Table 4** Performance comparison of different prediction models by CNN and LSTM methods

| Univariate predication model | | | | | |
|---|---|---|---|---|---|
| Indicator and method | | MAE | RMSE | MAPE | $R^2$ |
| Cumulative energy | LSTM | 2,557,425 | 4,746,242 | 4.54 | 0.980 |
| | CNN | 3,283,243 | 4,934,981 | 5.54 | 0.978 |
| Cumulative apparent volume | LSTM | 253,407 | 301,422.2 | 7.29 | 0.974 |
| | CNN | 255,395.1 | 362,784.9 | 7.74 | 0.962 |
| Cumulative event number | LSTM | 7.75 | 11.13 | 9.75 | 0.953 |
| | CNN | 5.09 | 6.89 | 5.62 | 0.982 |
| Multiple input series model | | | | | |
| Indicator and method | | *MAE* | *RMSE* | *MAPE* | $R^2$ |
| Rockburst probability | LSTM | 0.060 | 0.091 | 29.84 | 0.753 |
| | CNN | 0.043 | 0.072 | 19.05 | 0.847 |
| Multiple parallel series model | | | | | |
| Indicator and method | | *MAE* | *RMSE* | *MAPE* | $R^2$ |
| Cumulative apparent volume | LSTM | 359,178.25 | 467,749.82 | 10.98 | 0.937 |
| | CNN | 240,241.77 | 335,013.36 | 8.12 | 0.968 |
| Energy index | LSTM | 0.065 | 0.087 | 78.69 | 0.611 |
| | CNN | 0.054 | 0.084 | 74.22 | 0.644 |

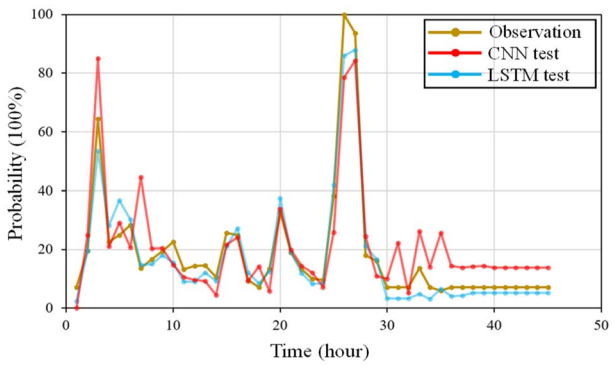


**Fig. 20** Comparison of multiple input series models with CNN and LSTM networks

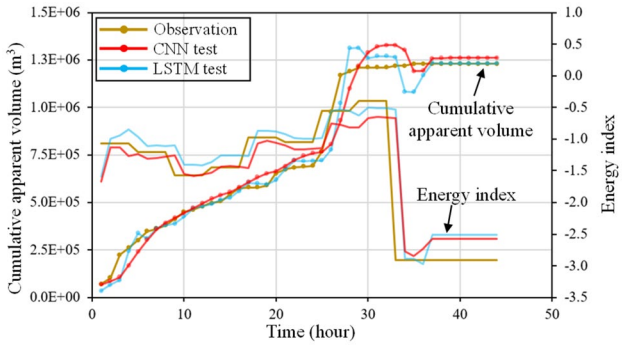


**Fig. 21** Comparison of multiple parallel series models with CNN and LSTM networks

of the two models is relatively poor in terms of the energy index, as the $R^2$ coefficient of the CNN model is only 0.644, which is due to the large fluctuation in the energy index curve. However, the test curves of the energy index of the two models are consistent with the trend in the observed curve, indicating that the evolution of the energy index curve can be predicted by the models.

## 4.2 Rockburst Risk Interpretation Based on Microseismic Time Series Prediction

In the above section, we used a trained model to test the microseismic data collected in the complete process of rockbursts, and the model performance was validated by comparing the test curve with the observation curve. Here, we make some new attempts to apply the prediction model of the microseismic multivariate time series. In this case, the prediction curve of the microseismic multi-parameters is inferred from the observation curve. The input samples for the models come from the values observed at the beginning. As the prediction curve extends, more predictive values are gradually added to the input sample until the predictive values fill the input sample. This is consistent with the application scenario of the time series prediction model presented in Sect. 2.

1. Prediction Made by Univariate Time Series Model and Interpretation of Rockburst Risk

   The untrained data pertaining to the "12.17" rockburst were selected for the prediction using the univariate time

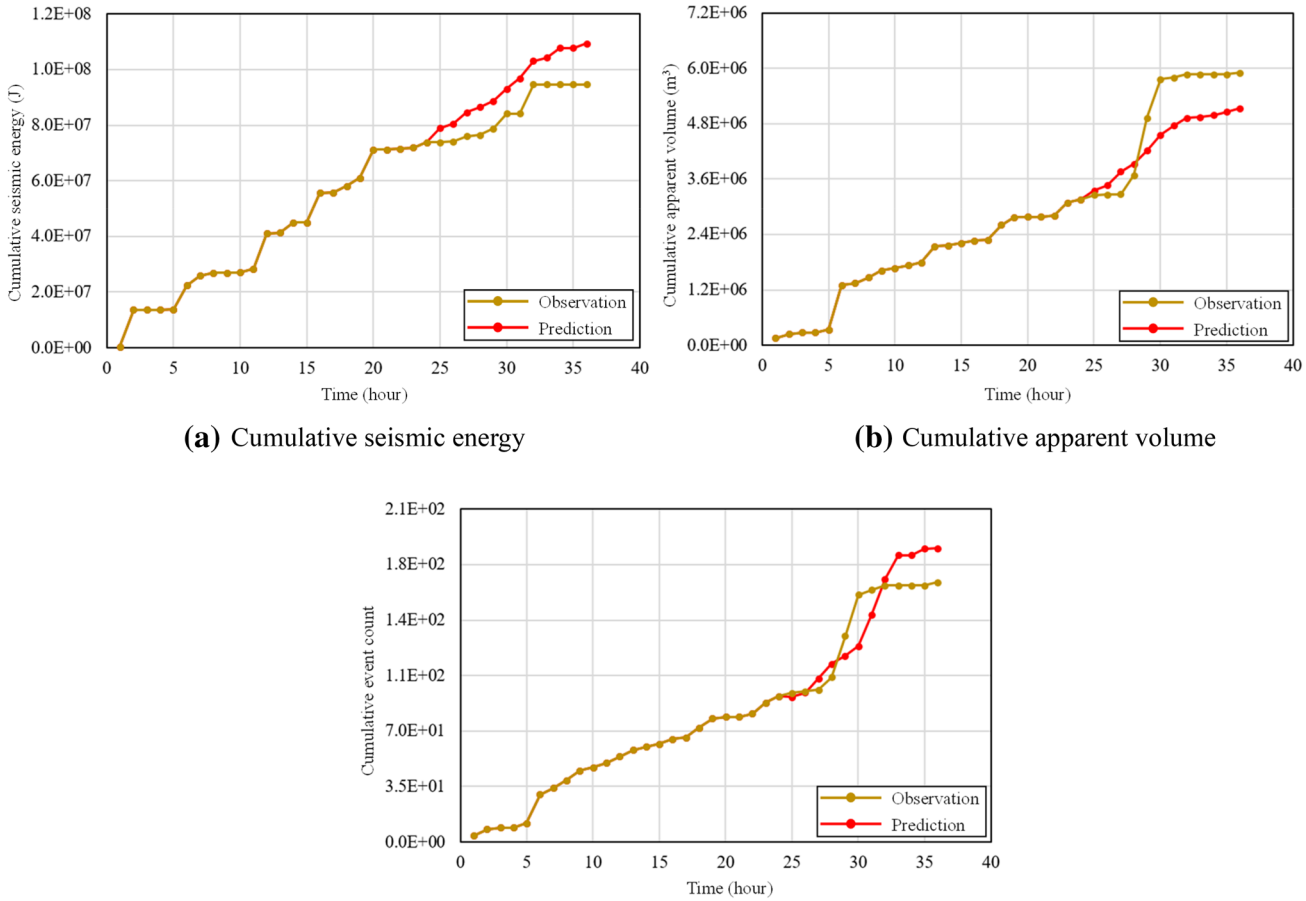


**Fig. 22** Prediction result of univariate model and interpretation of rockburst risk

series model. As shown in Fig. 22, the predicted time period lasts 11 h, which is from the 25th hour before the rockburst to the 36th hour after the rockburst (rockburst occurred at the 30th hour). In the prediction of the microseismic values at the 25th hour, the input sample is from the observation sequence. For the subsequent microseismic parameter prediction at each hour, the input sample should gradually include more previous predictive values. Although there are some differences between the prediction and observation curves, their evolution trends are the same. The cumulative energy, cumulative event number, and cumulative apparent volume before rockburst occurrence increase quickly with a steep-shaped curve, indicating that the risk of a rockburst increases gradually. After the rockburst, the growth of each index becomes slower, and a gentle step appears in the curve.

2. Prediction Made by the Multiple Input Series Model and Interpretation of Rockburst Risk

Figure 23 shows the prediction result of the evolution of the "12.17" rockburst, obtained using the multiple input series model. The input to the model comes from the observed and predicted values of the three variables, namely the cumulative apparent volume, cumulative event number, and cumulative energy, and the output is

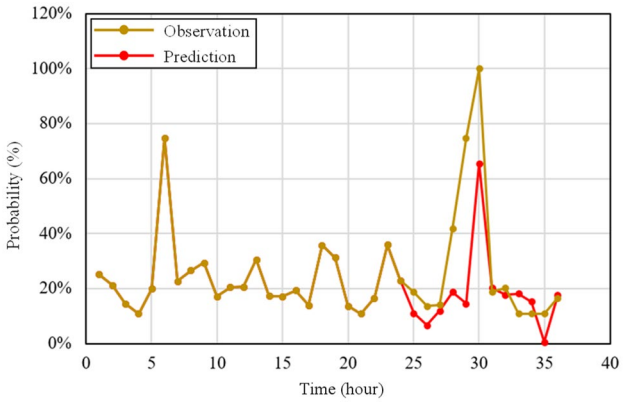


**Fig. 23** Prediction result of multiple input series model and interpretation of rockburst risk

the index evolution of the rockburst probability in the future time period. The diagram shows that the prediction curve of the rockburst probability fluctuates significantly, mainly because the training sample of this index also exhibits a significant fluctuation. Although the predicted curve of the index is different from the real value, their evolution trends are in good agreement, indicating that the index continues to increase and reaches the highest fluctuation point before rockburst occurrence.

3. Prediction Made by Multiple Parallel Series Model and Interpretation of Rockburst Risk

Figure 24 shows the prediction result of the "12.17" rockburst evolution, obtained using the multiple parallel series model. The input to the model comes from the observed and predicted values of the cumulative apparent volume and energy index. The output is the index evolution of the future time period corresponding to the two variables. The diagram shows that the prediction curves of the cumulative apparent volume and energy index are slightly different from their observation curves. The prediction curve of the cumulative apparent volume growth is ahead of its observation curve, and the decrease in the energy index in the prediction curve lags behind that in the observation curve. The predicted value is in good agreement with the evolution trend in the real value, indicating that the cumulative apparent volume increases significantly and that the energy index decreases rapidly before rockburst occurrence. The model can predict and infer the rockburst risk in advance.

Unlike conventional methods that focus on predicting the potential rockburst grade, the proposed method can theoretically provide a time tag for rockburst risk assessment. The specific implementation process involves training the model with isochronized microseismic data obtained during a rockburst, and their evolution trends in the future are obtained using the moving-window method. Some microseismic indices (e.g., rockburst probability and energy index) have evident characteristics during a rockburst. Therefore, the time series prediction method proposed in this paper combines the future evolution trends of these indices to better interpret rockburst risk (and not by simply using the current state or values of the indices, in which case the result may be one-sided due to curve fluctuation). Moreover, using the deep convolution neural network method for the time series prediction of the microseismic multi-parameters is simple a choice preference. The LSTM neural network was used for a comparative study. In fact, any deep learning method that can reflect the mapping relationship between the existing observation sequence and the future prediction sequence is feasible. Thus, this paper provides an effective strategy for rockburst prediction based on data related to microseismic activity.

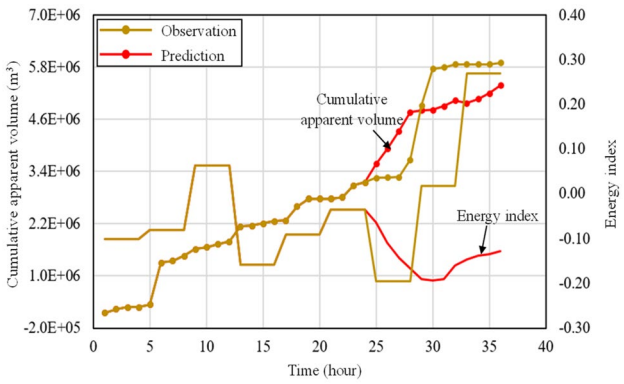


**Fig. 24** Prediction result of multiple parallel series model and interpretation of rockburst risk

## 5 Conclusion

In this study, the evolution prediction of microseismic parameters based on a deep learning method was explored to evaluate the risk of rockbursts in deep underground engineering construction. Various prediction models of the microseismic univariable and multivariable based on different microseismic parameters are proposed, including a univariate prediction model, multiple parallel series model, multiple input series model, and multivariate multi-step prediction model. The results of model tests and comparative analyses show that the CNN-based models can accurately predict evolution trends in microseismic parameters and are generally better than the LSTM-based models. By deducing the prediction curves of the microseismic parameters from the predicted values as the input sample, we found the prediction curve to be in good agreement with the real curve. This proves that the selected microseismic parameters, including the cumulative energy, cumulative apparent volume, cumulative event number, rockburst probability, and energy index, are effective and reasonable for time series prediction. The proposed method has the potential to predict and infer rockburst risk in advance. In addition, the time series prediction model of the microseismic multi-parameters can be combined with a quantitative early warning model to form an integrated model for rockburst prediction and early warning. The proposed method can help reveal the evolution trends in the key characteristics associated with future rockburst development and provide an effective technical means for the prediction and early warning of rockbursts in the field of deep underground and mining engineering. The proposed method can also be applied to the prediction of other types of geological disasters using other appropriate indicators.

**Acknowledgements** We sincerely thank the owners and construction staff of the Micangshan tunnel of the Sichuan–Shaanxi expressway who provided kind support in a dangerous construction environment with the risk of high-stress hazards. This work was financially supported by the National Natural Science Foundation of China (grant numbers 41807255 and 42177173); State Key Laboratory of Geohazard Prevention and Geoenvironment Protection Independent Research Project (grant numbers SKLGP2020Z010); and Sichuan Science and Technology Project (grant number 2019YJ0465).

## References

Andy HW, Andrew S, Duan Y, Luo X (2020) Identifying microseismic events in a mining scenario using a convolutional neural network. Comput Geosci 137:104418

Anita Y, Jha CK, Aditi S (2020) Optimizing LSTM for time series prediction in Indian stock market. Proc Comput Sci 167:2091–2100

Bashar A, Maysam A (2020) A new hybrid financial time series prediction model. Eng Appl Artif Intell 95:103873

Dai F, Li B, Xu NW, Zhu YG (2017) Microseismic early warning of surrounding rock mass deformation in the underground powerhouse of the houziyan hydropower station, china. Tunn Undergr Space Tech 62:64–74

De Santis F, Contrucci I, Kinscher J, Bernard P, Renaud V, Gunzburger Y (2019) Impact of geological heterogeneities on induced-seismicity in a deep sublevel stoping mine. Pure Appl Geophys 176(2):697–717

Dip AC, Giroux B, Gloaguen E (2021) Microseismic monitoring of rockbursts with the ensemble Kalman filter. Near Surf Geophys 19(4):429–445

Dong LJ, Johan W, Potvin Y, Li XB (2016) Discrimination of mine seismic events and blasts using the fisher classifier, naive bayesian classifier and logistic regression. Rock Mech Rock Eng 49(1):183–211

Dou LM, Cai W, Cao AY, Guo WH (2018) Comprehensive early warning of rock burst utilizing microseismic multi-parameter indices. Int J Min Sci Technol 28:767–774

Feng GL, Feng XT, Chen BR, Xiao YX, Yu Y (2015) A microseismic method for dynamic warning of rockburst development processes in tunnels. Rock Mech Rock Eng 48(5):16

Feng XT, Xiao YX, Feng GL, Yao ZB, Chen BR, Yang CX, Su GS (2019) Study on the inoculation process of rockburst. Chin J Rock Mech Eng 598(04):649–673 (**in Chinese**)

Feng GL, Chen BR, Jiang Q, Xiao YX, Li PX (2021) Excavation-induced microseismicity and rockburst occurrence: similarities and differences between deep parallel tunnels with alternating soft-hard strata. J Cent South Univ 28:582–594

Hou Y, Xie B, Liu H (2019) Bayesian regularization neural network model for stock time series prediction. Int J Perform Eng 15(12):3271–3278

Hu SH, Tan YL, Ning GJ, Guo WY, Liu XS, Caliò I (2017) Multiparameter monitoring and prevention of fault-slip rock burst. Shock Vib 2017:7580109

Ji B, Xie F, Wang XP, He SQ, Song DZ (2020) Investigate contribution of multi-microseismic data to rockburst risk prediction using support vector machine with genetic algorithm. IEEE Access 8:58817–58828

Jiang RC, Dai F, Liu Y, Wei MD (2020) An automatic classification method for microseismic events and blasts during rock excavation of underground caverns. Tunn Undergr Space Technol 101:103425

Kumar V, Gopalakrishnan N, Singh NP, Cherukuri S (2019) Microseismic monitoring application for primary stability evaluation of the powerhouse of the Tapovan Vishnugad Hydropower Project. J Earth Syst Sci 128:169

Li Y, Yang TH, Liu HL, Wang H, Hou XG, Zhang PH, Wang PT (2016) Real-time microseismic monitoring and its characteristic analysis in working face with high-intensity mining. J Appl Geo 132:152–163

Li PX, Feng XT, Feng GL, Xiao YX, Chen BR (2019a) Rockburst and microseismic characteristics around lithological interfaces under different excavation directions in deep tunnels. Eng Geol 260:105209

Li TB, Liu TY, Chen GQ, Ma CC, Zhang H (2019b) Construction of highway tunnel microseismic monitoring system and analysis of microseismic characteristics. J Undergr Space Eng 15(04):1188–1196

Liang WZ, Asli S, Zhao GY, McKinnon SD, Wu H (2020) Short-term rockburst risk prediction using ensemble learning methods. Nat Hazards 104:1923–1946

Liu C, Li SG, Cheng C, Cheng XY (2017a) Identification methods for anomalous stress region in coal roadways based on microseismic information and numerical simulation. Int J Min Sci Technol 27(3):525–530

Liu C, Li SG, Cheng C, Xue JH (2017b) Activation characteristics analysis on concealed fault in the excavating coal roadway based on microseismic monitoring technique. Int J Min Sci Technol 27(05):883–887

Liu F, Ma TH, Tang CA, Chen F (2018) Prediction of rockburst in tunnels at the jinping ii hydropower station using microseismic monitoring technique. Tunn Undergr Space Tech 81:480–493

Liu F, Tang CA, Ma TH, Tang LX (2019) Characterizing rockbursts along a structural plane in a tunnel of the hanjiang-to-weihe river diversion project by microseismic monitoring. Rock Mech Rock Eng 52:1835–1856

Ma CC, Li TB, Zhang H, Han YX, Zhou XH (2019) Preliminary study on stiffness effect of support system with microseismic characteristics of rockburst. Chin J Rock Mech Eng 38(S1):2976–2987 (**in Chinese**)

Ma CC, Li TB, Zhang H (2020) Microseismic and precursor analysis of high-stress hazards in tunnels: a case comparison of rockburst and fall of ground. Eng Geol 265(1):105435

Polson NG, Sokolov VO (2017) Deep learning for short-term traffic flow prediction. Transp Res C Emer 79:1–17

Pu YY, Derek BA, Liu V, Mitri H (2019) Machine learning methods for rockburst prediction-state-of-the-art review. Int J Min Sci Technol 29(4):565–570

Pu YY, Derek BA, Robert H (2020) Using machine learning approach for microseismic events recognition in underground excavations: Comparison of ten frequently-used models. Eng Geol 268:105519

Shang XY, Li XB, Peng K, Wang ZW, Weng L (2017) Application of FSWT-SVD model to feature extraction of microseismic signals of rock mass. Shock Vib 36(14):52–60

Song EW, Frank KS, Kang HG (2017) Effective spectral and excitation modeling techniques for lstm-rnn-based speech synthesis systems. IEEE/ACM Trans Audio Speech Lang Process (TASLP) 25(11):2152–2161

Srinivasan C, Arora SK, Benady S (1999) Precursory monitoring of impending rockbursts in Kolar gold mines from microseismic emissions at deeper levels. Int J Rock Mech Min 36(7):941–948

Tan YL, Yin YC, Gu ST, Tian ZW, Liu SM (2015) Multi-index monitoring and evaluation on rock burst in yangcheng mine. Shock Vib 2015:624893

Thomas F, Christopher K (2018) Deep learning with long short-term memory networks for financial market predictions. Eur J Oper Res 270(2):654–669

Wöllmer M, Schuller B, Eyben F, Rigoll G (2010) Combining long short-term memory and dynamic bayesian networks for

incremental emotion-sensitive artificial listening. IEEE J Sel Top Signal Process 4(5):867–881

Xiao PW, Li TB, Xu NW, Zhou Z, Liu XH (2019) Microseismic monitoring and deformation early warning of the underground caverns of Lianghekou hydropower station, Southwest China. Arab J Geosci 12(16):496

Xue RX, Liang ZZ, Xu NW, Dong LL (2020) Rockburst prediction and stability analysis of the access tunnel in the main powerhouse of a hydropower station based on microseismic monitoring. Int J Rock Mech Min 126:104174

Zhang JL, Sheng GQ (2020) First arrival picking of microseismic signals based on nested U-Net and Wasserstein Generative Adversarial Network. J Petrol Sci Eng 195:107527

Zhang H, Ma CC, Pazzi V, Zou YL, Casagli N (2020a) Microseismic signal denoising and separation based on fully convolutional encoder–decoder network. Appl Sci 10:6621

Zhang H, Ma CC, Pazzi V, Li TB, Casagli N (2020b) Deep convolution neural network for microseismic signal detection and classification. Pure Appl Geophys 177(12):1–17

Zhang SC, Ma TH, Tang CA, Jia P, Wang YC (2020c) Microseismic monitoring and experimental study on mechanism of delayed rockburst in deep-buried tunnels. Rock Mech Rock Eng 53:2771–2788

Zhang YG, Yan BB, Memon A (2020d) A novel deep learning framework: Prediction and analysis of financial time series using CEEMD and LSTM. Expert Syst Appl 159:113609

Zhao Y, Yang TH, Marco B, Zhang PH, Yu QL, Zhou JR, Liu FY (2018) Study of the rock mass failure process and mechanisms during the transformation from open-pit to underground mining based on microseismic monitoring. Rock Mech Rock Eng 51(5):1473–1493

Zhou J, Shi XZ, Huang RD, Qiu XY, Chen C (2016) Feasibility of stochastic gradient boosting approach for predicting rockburst damage in burst-prone mines. Trans Nonferrous Metal Soc 26(7):1938–1945